Effect of Molecular Dynamics Water Models on Flux, Diffusivity, and Ion Dynamics for Polyamide Membrane Simulations

Suwei Liu[a], Sinan Keten[a,b] and Richard M. Lueptow[a,c,d,*]

[a]Department of Mechanical Engineering, Northwestern University, Evanston, IL, USA
[b]Department of Civil and Environmental Engineering, Northwestern University, Evanston, IL, USA
[c]Department of Chemical and Biological Engineering, Northwestern University, Evanston, IL, USA
[d]The Northwestern Institute on Complex Systems (NICO), Northwestern University, Evanston, IL, USA

ARTICLE INFO

Keywords:
Molecular dynamics
Water model
SPC/E, TIP3P, TIP4P
Water filtration membrane
Ion dynamics

ABSTRACT

While molecular dynamics (MD) models for reverse osmosis (RO) and nanofiltration (NF) membranes are useful for studying water filtration processes, the specific water model and force-field parameters have a profound impact on key measures such as flux and diffusivity. Moreover, ensemble related parameters such as temperature and how it is controlled via a thermostat also affect simulation results. To quantify these effects, we investigate the performance of three commonly used water models, SPC/E, TIP3P, and TIP4P, in simulating an NF membrane system at varying temperatures and thermostat settings. All three water models successfully capture the Arrhenius relationship between water diffusivity and temperature as well as the linear relationship between water flux through the membrane and water diffusivity in the membrane. However, SPC/E underpredicts, TIP3P overpredicts, and TIP4P most accurately reproduces the water dynamics, especially water self-diffusivity, compared to experiments. We also investigate the effect of the water model on common salt solutions at various concentrations. TIP4P generally outperforms the other two water models when describing ion diffusivities and water solvation shells around ions. These findings indicate that TIP4P is an appropriate water model to use in polyamide membrane MD simulations.

1. Introduction

Molecular dynamics (MD) is emerging as a powerful approach to probe membrane filtration at the Ångström scale, a level that experiments and models cannot resolve [1, 2]. Over the past two decades, a number of MD simulation studies have been performed for polyamide based membranes (Table 1), primarily focusing on reverse osmosis (RO) membranes of trimesoyl chloride (TMC) polymerized with m-phenylene diamine (MPD), with a limited number considering nanofiltration (NF) membranes of TMC polymerized with piperazine (PIP). These atomistic scale simulations provide information that is very difficult to obtain experimentally. For example, it is difficult to measure the porosity and density of NF membranes, since their active layers are usually less than 100 nm thick [3]. Yet MD studies of RO and NF membranes can easily provide density and pore size characterizations that can be used to connect transport observations and continuum models to atomic-scale interactions. Trajectories of water molecules or solutes can be tracked as they diffuse through the membrane, and membrane dynamics, including positions of charged functional groups and solutes, can be resolved with sub-nanometer and sub-picosecond resolution.

One of the challenges in studying membrane filtration processes using MD is that the results depend on the force-fields and simulation conditions used in the MD simulations. The force-fields represent both the interactions of interatomically bonded atoms and the non-bonded forces between atoms, including van der Waals and electrostatic forces. Accurate simulation results depend on the ability of the MD force-fields to correctly represent these Ångström scale forces. A complete set of force-field parameters necessary to simulate molecules includes bond lengths, bond angles, atomic partial charges, and parameters describing Lennard-Jones potentials. In addition, operating conditions like temperature are regulated using "thermostats" to introduce or dissipate energy from a system in MD simulations.

Crucial to studies of membrane filtration is the appropriate MD model to use for the water molecule. Our goal in this paper is to examine how the specific water model that is used affects MD simulation results at different temperatures for a typical polyamide membrane system. Specifically, we consider the effect of different MD water models on the water diffusion, solute diffusion, and water flux in an NF membrane.

Although water is a commonly simulated molecule with a simple atomic structure, accurate force-field parametrization of water is challenging. At least 30 MD water models have been developed over the past 40 years, each with its own characteristics [4]. A variety of water models have been considered for a wide range of applications including SPC [5], SPC/E [6], SPC/Fw [7], TIP3P [8], TIP4P [8, 9] and TIP5P [10]. Here, SPC refers to Simple Point Charge, and TIP refers to Transferable Interaction Potential. The number in any of the abbreviations refers to the number of "sites" in the water model. At a minimum, there are three sites for water, corresponding to two hydrogen atoms and one oxygen atom (for example, TIP3P and SPC models). When there are more than three sites, the additional sites correspond

*Principal corresponding author
r-lueptow@northwestern.edu (R.M. Lueptow)
orcid(s): 0000-0002-1855-1471 (R.M. Lueptow)

Table 1
MD membrane studies performed in the 2000s.

Water Model	Polymer Type	Temperature (K)	Thermostat Setting	Reference
SPC	RO (TMC + MPD)	300	Nosé-Hoover	Xiang *et al.* [16–18]
SPC	RO (TMC + MPD)	298	Berendsen, Velocity Rescaling (τ = 0.1 ps)	Kolev and Freger [19]
SPC/E	RO (TMC + MPD)	300	Nosé-Hoover	Muscatello *et al.* [20]
TIP3P	RO (TMC + MPD)	300	Nosé-Hoover	Harder *et al.* [21]
TIP3P	RO (TMC + MPD)	298	Velocity Rescaling	Kolev and Freger [22]
TIP3P	RO (TMC + MPD)	300	Langevin	Luo *et al.* [23]
TIP3P	RO (TMC + MPD)	300	Langevin	Shen *et al.* [24, 25]
TIP3P	RO (TMC + MPD)	300	*Not Reported*	Zhang *et al.* [26]
TIP3P	RO (TMC + MPD)	298	Nosé-Hoover	Jahan Sajib *et al.* [27]
TIP3P	NF (TMC + PIP)	300	Langevin (γ = 1 ps^{-1})	Liu *et al.* [28]
TIP3P	RO (TMC + MPD)	300	Velocity Rescaling	Zhang *et al.* [29]
TIP4P-Ew	RO (TMC + MPD)	300	Nosé-Hoover (τ = 1 ps)	Hughes and Gale [30, 31]
TIP4P/2005	RO (TMC + MPD)	300	Nosé-Hoover	Ding *et al.* [32–35]
TIP4P/2005	RO (TMC + MPD)	300	*Not Reported*	Liyana-Arachchi *et al.* [36]

to dummy atoms, sometimes called a "lone pair," referring to a pair of valence electrons in a molecule not shared with another atom via a covalent bond, that have charge but no mass. The additional sites are used to improve the electrostatic charge distribution of the water model to better reflect the polar nature of a water molecule. Various water models are used to accurately simulate specific properties of bulk water, e.g., solid water (ice), surface tension, or dielectric constants [4]. Similarly, the interactions of the water molecules with other molecules in the system, for instance charged solutes or polyamide membrane structures considered here, need to be taken into account. Of course, MD simulations are based on the interatomic potentials between all the atoms that are simulated. As a result, a 4-site water model has more computational overhead than a 3-site water model. The desired situation is to use the water model that most accurately reflects the physical situation that is being modeled at the lowest computational cost.

Previous studies comparing water models have focused on physical properties in water-only systems. For example, Mark and Nilsson [11] find significant differences in self-diffusion and Zielkiewicz [12] notes differences in the energy and lifetime of hydrogen bonds between water models. A handful of studies consider the impact of the water model on water transport in various porous systems. Prasad *et al.*, [13] find that the water flux in graphene nanopore systems depends on the water model that is used due to differences in hydrogen bond dynamics, partial charge, and diffusion. Likewise, Liu and Patey [14] show that the water flux in carbon nanotubes varies depending on the different water model with the origin of the differences due to different ordering of water molecules as they flow through the nanotube. Srivastava *et al.* [15] note that water models behave differently in the interfacial regions in aqueous lipid bilayer systems due to differences in diffusivity and hydrogen bond breaking.

As indicated in the first column of Table 1, various water models have been used in MD simulations of polyamide-based RO and NF membranes, but we are unaware of any studies comparing the impact of the water model on the simulation results. The water models that are used fall into the categories of SPC (SPC/E), TIP3P, and TIP4P (TIP4P-Ew and TIP4P/2005). As shown in Fig. 1(a), SPC/E and TIP3P share the same structure of a 3-atom rigid planar model. TIP4P, shown in Fig. 1(b), is a 4-site rigid planar model. In addition to one oxygen atom and two hydrogen atoms, a mass-less site is added to carry the negative charge while the oxygen atom stays neutral.

Figure 1: Water model illustrations for (a) SPC/E, TIP3P, and (b) TIP4P, where red beads are oxygen atoms, white beads are hydrogen, and the green bead has zero mass but carries a charge in TIP4P. (Color online.)

We also note the thermostats that are used to maintain the temperature, either 298 K or 300K, for previous MD simulations of membranes in Table 1. While temperature has a macroscopic effect on water transport through a membrane, the temperature on the molecular level is defined by the average kinetic energy of all the atoms in the system in the canonical ensemble (NVT, where the amount, N, volume, V, and temperature, T, are constant). The temperature is regulated by a thermostat, which allows energy to enter or dissipate from the system during simulations by modifying atoms' velocities. For the simulations listed in Table 1, common thermostat types are Nosé-Hoover [37–39] (extended system), Berendsen [40] (weak coupling), Langevin [41] (stochastic), and velocity rescaling [42] (strong coupling). These thermostats deploy various

algorithms to regulate temperature. For example, extended system thermostats contain an additional degree of freedom associated with the constant temperature, weak coupling methods scale the velocity in the direction of the desired temperature, stochastic methods randomly assign new velocities to certain atoms to reach the target temperature, and strong coupling methods scale the velocity to exactly render the desired temperature. The MD simulations described in this study use a simulation package called Nanoscale Molecular Dynamics (NAMD) [43]. Within NAMD, the use of the Langevin thermostat enables parallel scalability better than Nosé-Hoover thermostat [44]. Hence, we use the Langevin thermostat in this study rather than other temperature control methods.

After describing the simulation methods in the next section, we first consider how the water models affect membrane properties, focusing on membrane density, pore size distribution, mean pore diameter, and percolated free volume. Next, we examine the influence of water models on water transport in terms of water diffusivity, both outside and inside the membrane, and water flux through the membrane at temperatures from 283 K to 313 K. We also measure the effect of the damping for the Langevin thermostat on the water flux for the three water models. Then we examine the effect of the water model on water diffusivity in the presence of ionic solutes (Na^+, K^+, Mg^{2+}, Ca^{2+}, and Cl^-) as well as the effect of the water model on solute diffusivity at various solute concentrations. We conclude with comments about the suitability of the three water models for various membrane simulation conditions.

2. Methods

Similar to our previous simulations [28], we use the NAMD simulation package [43] along with general AMBER forcefields (GAFF) [45]. The SHAKE algorithm [46] with a cutoff of the non-bonded potential of 9 Å is used to constrain the bond between each hydrogen and its mother atom. The Particle Mesh Ewald (PME) method [47] is used to compute full electrostatics with a grid spacing of 1 Å. For all simulations in this study, the time step is set at 1 fs with output saved every 2 ps.

2.1. Water models

Force-field parameters used to calculate bonded and non-bonded energies MD simulations are summarized in Table 2 for the three water models considered in this study. The spring constants (K_b, K_θ) describing strength of bonded energies, equilibrium bond length (b_0), and equilibrium angle (θ_0) are used to calculate bonded energy terms. For non-bonded energies, atom partial charges (q) for oxygen (O), hydrogen (H), and the lone pair (LP) are used to calculate the Coulombic or electrostatic potential according to

$$V_{\text{elec}}(r_{ij}) = \frac{q_i\, q_j}{r_{ij}}. \tag{1}$$

For short-range interactions, the Lennard-Jones (LJ) potential is evaluated using

$$V_{\text{LJ}}(r) = 4\varepsilon \left(\left(\frac{r_0}{r}\right)^{12} - \left(\frac{r_0}{r}\right)^{6} \right), \tag{2}$$

where ε describes the energy well-depth and r_0 is the distance between two non-bonded atoms when V_{LJ} is at its minimum.

Table 2
Bonded, electrostatic, and nonbonded parameters of SPC/E, TIP3P, and TIP4P water models.

Param.	Units	SPC/E[6]	TIP3P[48]	TIP4P[8]
K_b^{OH}	$kcal\ mol^{-1} Å^{-2}$	450.0	450.0	450.0
b_0^{OH}	$Å$	1.0	0.9572	0.9572
K_θ^{HOH}	$kcal\ mol^{-1} rad^{-2}$	55.0	55.0	55.0
θ_0^{HOH}	deg	109.47	104.52	104.52
q^O	e	-0.8476	-0.834	0
q^H	e	0.4238	0.417	0.52
q^{LP}	e	*N/A*	*N/A*	-1.04
ε^{OO}	$kcal\ mol^{-1}$	0.1553	0.1521	0.155
r_0^{OO}	$Å$	3.5256	3.5256	3.5398
ε^{HH}	$kcal\ mol^{-1}$	0	0.046	0
r_0^{HH}	$Å$	0	0.449	0

2.2. Water transport simulation

Here we use a mixed aromatic-aliphatic piperazine-based polyamide NF membrane model corresponding to pH ≈ 10, unless otherwise noted, to consider water-membrane interactions within a highly charged membrane. This membrane model is one of 56 distinct NF membrane models that we previously investigated [28]. In addition to different physical properties (primarily membrane density), the membrane model realizations in that study have varying concentrations of negatively charged functional groups (COO^-), which are related to specific feed pH values based on experimental studies of COO^- concentration at different feed pH values [49, 50]. For the size of the membrane simulated here (52 × 52 × 40 $Å^3$), 30 COO^- functional groups corresponds to a 0.5 M charge concentration in the membrane. In our previous study we indicated that this concentration corresponds to pH ≈ 11 based on data for a similar NF membrane [49], but new data for a PIP-based FilmTec™ NF270 that is now available [50] indicates a better estimate is pH ≈ 10. We further note that our previous study indicates that membrane charge influences flux indirectly through its effect on membrane density and swelling. [28], but we consider a highly charged membrane here to assure that the membrane charge and polar nature of the water molecule are adequately addressed. To assure that the membrane charge does not affect the comparison between water models, we also perform several simulations

for a membrane with pH ≈ 7 (14 COO^- functional groups, 0.23 M charge concentration).

Since the impact of the specific water model used in a simulation is investigated here, it is necessary to initially hydrate the dry membrane with the water model being considered: SPC/E, TIP3P, or TIP4P. The membrane hydration setup consists of a dry membrane bounded by two equal-sized water reservoirs, each with 15 Na^+ counterions to balance the membrane charge. Graphene sheets, to which a force can be applied to pressurize the system, bound the outer portion of each reservoir [28], see Fig. 2. The hydration process involves two pressure settings on the graphene sheets. The pressure on the graphene sheets is first set to $P_1 = P_2 = 30$ MPa for 5 ns to drive water molecules into the membrane from either reservoir. The pressure is then lowered to $P_1 = P_2 = 0.1$ MPa to further allow the diffusion of water molecules and Na^+ counterions into the membrane. Details of membrane hydration are available in our previous study [28].

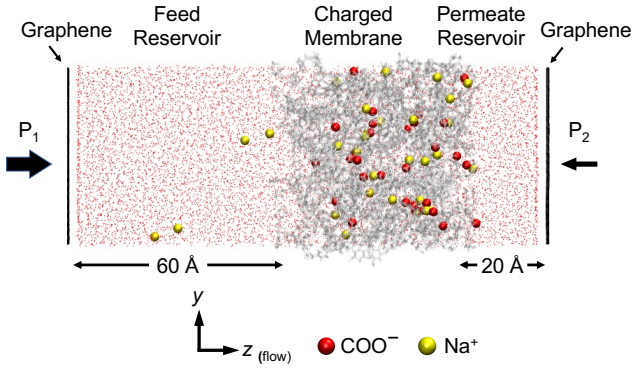

Figure 2: Simulation setup. Water molecules are red points (not related to water's actual size), graphene sheets are black, membrane atoms are gray, carboxyl sites are labeled as red beads, and counterions are yellow beads. (Color online.)

The fully hydrated and equilibrated membrane is used for non-equilibrium MD simulations of water transport, as shown in Fig. 2. The system consists of the hydrated membrane with Na^+ counterions between two water reservoirs that are bounded by graphene sheets to apply pressure to force water transport through the membrane. The dimensions of the graphene sheets, the feed reservoir, and the permeate reservoir are non-periodic in the z-direction, and match the dimensions of the membrane in the x- and y-directions with periodic boundary conditions. The feed reservoir is 60 Å in z-direction and the permeate reservoir is 20 Å in z-direction. The system box size in all directions is kept constant throughout the entire simulation. A pressure of $P_1 = 150$ MPa is applied to the left graphene sheet while a back pressure of $P_2 = 0.1$ MPa is applied to the right one. This pressure difference mimics the actual filtration process, although the transmembrane pressure is two orders of magnitude larger than a typical NF membrane operating pressure [3]. The high operating pressure for the simulations is necessary in order to observe significant transport on nanosecond timescales. All water transport simulations are run for 20 ns, which is the same as our previous study [28]. This duration is sufficient to observe the linear relationship between the number of water molecules passing through the membrane and time (i.e., constant flux) with a computational cost (about 1-day wall clock time per simulation) that is acceptable. We also validate in our previous study that the resulting MD simulation water flux is consistent with experimental values measured for NF membranes at normal operating pressures [28]. To allow the membrane to dynamically evolve during water transport without being displaced due to the large pressure difference, roughly 10% of the atoms in the y-z plane at the periodic boundaries of the membrane are fixed in space.

In addition to investigating the effect of water models on water diffusion and flux, we also consider the roles of system temperature and the Langevin thermostat setting (Langevin damping coefficient, γ). Three temperatures, 283 K, 300 K, and 313 K, representing the range of practical operating conditions, are used while keeping the Langevin damping coefficient constant ($\gamma = 1$ ps^{-1}, same as our previous study [28]). To accommodate statistical variation, 4 replicate simulations lasting 20 ns are performed for each temperature setting, and all atoms in each production run start with the same coordinates but different initial velocities. In addition, we consider 6 Langevin damping values from 0.01 ps^{-1} to 10 ps^{-1}, which include the commonly used Langevin damping values, 1 ps^{-1} to 5 ps^{-1} [51], in NAMD. The system temperature is set to 300 K for 4 replicate runs of all 6 cases. In total, we consider 108 independent simulations for various water models, temperatures, and Langevin damping values, each with a duration of 20 ns.

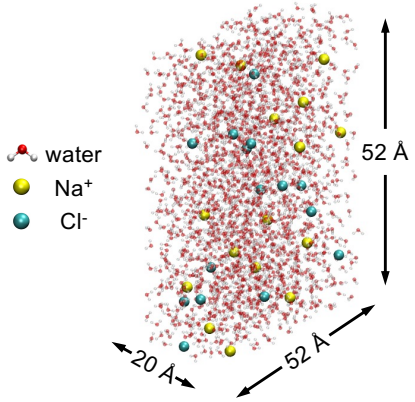

Figure 3: Ion diffusivity simulation setup for 0.5 M NaCl with TIP3P as water model. Simulation box is periodic in all directions; water molecule and ion representations are not-to-scale. (Color online.)

2.3. Ion dynamics simulation

In order to consider interactions between water models and various ions, we use a simplified MD system without a membrane, shown in Fig. 3. The solutes considered here are KCl, NaCl, $CaCl_2$, and $MgCl_2$, with long-range interactions based on Lennard-Jones and Coulombic terms to capture van

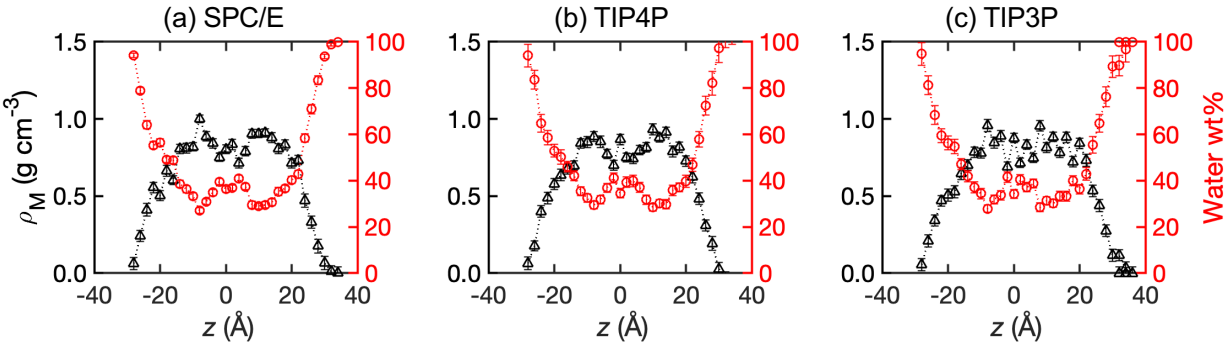

Figure 4: Membrane density, ρ_M (left vertical axis) and water wt% (right vertical axis) within the same pH ≈ 10 membrane model hydrated using (a) SPC/E, (b) TIP4P, and (c) TIP3P. (Color online.)

der Waals and electrostatic contributions [52]. The simulation box contains only one type of solute for each production run, and its x-, y-, and z-directions are all periodic, spanning 52 Å, 52 Å, and 20 Å, respectively. The dimensions are chosen to be similar to the water reservoir size in simulations that include a membrane and are large enough to prevent ions from interacting with their mirror image across the periodic boundary. We also consider different solute concentration levels, 0 M (pure water), 0.03 M, 0.06 M, 0.16 M, 0.25 M, 0.5 M (similar to the molarity of NaCl in seawater), and 1.0 M, to assure that solute-water interaction dynamics under both dilute and concentrated conditions are considered. Each production run is 10 ns at 300 K with $\gamma = 1$ ps^{-1} for a total of 75 independent simulations.

3. Results

3.1. Water model effect on membrane properties

We consider first the impact of the water models on the physical properties of a single membrane model (pH ≈ 10) that is hydrated with the three water models of interest here. The membrane density and water content in the membrane are calculated for 2 Å thick xy-slices of the membrane at z-locations spaced 2 Å apart and averaged over 2000 time instants separated by 2 ps during the last 4 ns of the equilibration at 300 K. As shown in Fig. 4, the membrane density, ρ_M, (left vertical axis) and water wt% (right vertical axis) are quite similar across the membrane thickness (z-direction) for the different water models. Despite similar density profiles, the average membrane densities within the densest region of the membrane differ slightly, with the density for the membrane hydrated using SPC/E a bit higher than those for TIP4P or TIP3P, as reported in Table 3.

The pore structure of the membrane model equilibrated using the different water models is characterized using PoreBlazer v4.0 through a geometric method that determines the pore size distribution (PSD) and the total free volume for a spherical "probe" of 0.25 Å. The pore size distributions averaged over 10 time instants separated by 0.4 ns during the last 4 ns of the equilibration are very similar for the three water models, as shown in Fig. 5. The percolated free volume (PFV), which is water-accessible volume within the membrane, is slightly more sensitive to the water model with which the membrane is hydrated, as indicated in Table 3. In short, based on the membrane density, PSD, and PFV, the TIP3P and TIP4P water models appear to swell the membrane slightly more than the SPC/E model, but the difference is not large.

Table 3
Average membrane density (ρ_M), percolated free volume (PFV), and membrane-water interaction energy for the same pH ≈ 10 membrane model hydrated using SPC/E, TIP4P, and TIP3P, along with their corresponding standard deviations.

	SPC/E	TIP4P	TIP3P
ρ_M (g·cm^{-3})	0.861 ± 0.004	0.829 ± 0.005	0.812 ± 0.005
PFV (%)	26.8 ± 1.3	29.7 ± 1.0	30.8 ± 2.3
Energy (kcal·mol^{-1})	-7.28 ± 0.60	-6.08 ± 0.47	-4.53 ± 0.87

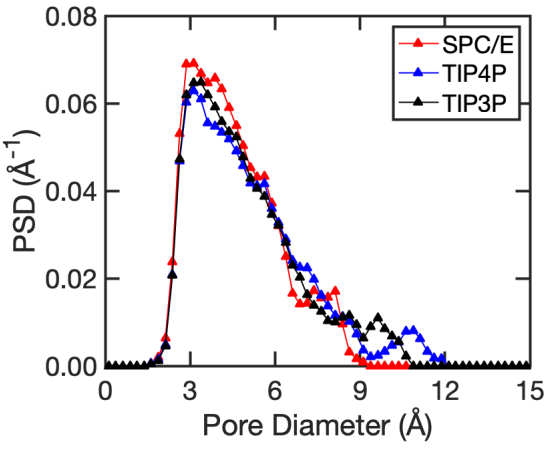

Figure 5: Pore size distribution (probe size = 0.25Å) for the same membrane model equilibrated with SPC/E (red), TIP4P (blue), and TIP3P (black).

To understand the slightly different effects that the water models have on the same membrane model, we consider the interaction energies between water molecules and the membrane nanostructure for water molecules enclosed within the membrane during the last 4 ns of the equilibration at 300 K. The interaction energies, which include electrostatic and van der Waals energies, are computed using the NAMDEnergy tool. The average interaction energies in Table 3 indicate that SPC/E has the most favorable interaction with the membrane followed by TIP4P and TIP3P. Furthermore, the larger interaction energy for SPC/E is consistent with a tighter hydrated membrane nanostructure (higher membrane density and lower PFV), followed by TIP4P and TIP3P. Similar results and trends occur for the pH ≈ 7 membrane. Thus, it appears that the membrane model can slightly alter the membrane nanostructure due to water-membrane interaction energy differences, although the effects are not large.

3.2. Water model effect on pure water dynamics

We first investigate the effect of temperature and Langevin damping parameters on water dynamics for the three water models in terms of water diffusivity and water flux through the membrane with an applied transmembrane pressure.

3.2.1. Water diffusivity

To quantify water dynamics, we measure water self-diffusivity, D_w, (both in the feed and permeate reservoirs, shown in Fig. 2) and the diffusivity of water inside the charged membrane, D_w^{mem}, during permeation. Measuring D_w allows a direct comparison to experimental values of D_w, while D_w^{mem} provides comparative information on the impact of the membrane nanostructure on reducing the water diffusivity for the different water models. The diffusivity is measured based on the mean square displacement (MSD) of water molecules at different time lag intervals τ, ranging from 2 ps (the highest resolution of our simulations) to 1 ns. The diffusion coefficient can be found from the relationship between the MSD and τ within the normal diffusion region [28].

As shown in Fig. 6(a), D_w (black data points) increases by 40% to 85% with an increase in temperature from 283 K to 313 K for all three water models, as would be expected. However, the differences between the three water models are significant. At 283 K, for instance, D_w simulated using TIP4P and TIP3P are twice and three times larger than SPC/E, respectively. Compared to experiments (red data points) [53–56], TIP4P best describes D_w among the water models considered here. We further note that previous simulations for SPC/E and TIP4P at 298 K [57] produced 67% and 31% larger values of D_w, respectively, than those found here, which are well over the experimental values. The differences with our simulations probably arise from a much smaller number of water molecules employed in this previous study, which necessitated the introduction of a correction term. Different thermostat settings and simulation packages might also explain the differences. These simulation-based differences further emphasize the challenges inherent in these types of simulations.

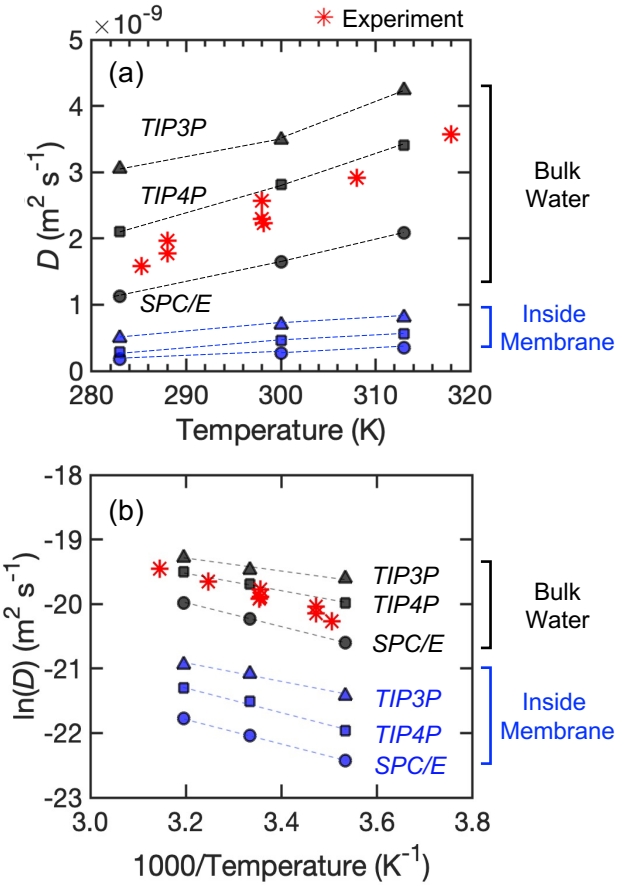

Figure 6: (a) Diffusion coefficient D as a function of temperature and (b) the corresponding Arrhenius plot for SPC/E (○), TIP4P (□), and TIP3P (△) water models and experimental data (∗) [53–56]. Black symbols indicate D_w, and blue symbols indicate D_w^{mem}. Each data point is an average of 4 replicate simulations and the standard error bars are generally the same size as the markers or smaller, so they are omitted for clarity. All simulations here use Langevin damping of $\gamma = 1$ ps^{-1}. (Color online.)

Similar trends for the three water models are also observed for D_w^{mem} [blue data points in Fig. 6(a)], although the diffusivity inside the membrane is much less than D_w because the membrane nanostructure constrains the motion of the water molecules [28]. The decrease in water mobility in the membrane can be expressed as the ratio, D_w/D_w^{mem}. This ratio averaged over 36 simulations is 6.03 ± 0.22, 6.19 ± 0.08, and 5.38 ± 0.10 for SPC/E, TIP4P, and TIP3P, respectively. The similar relatively large ratios suggest that the water model choice has little impact on the mobility of water in the membrane relative to that outside of the membrane, particularly given the similarities in the measures of the membrane properties in Table 3. Another way to consider this is that across all temperatures, the ratio of the diffusivities for the different water models are quite similar both inside (1.63 ± 0.06 for TIP4P to SPC/E and 2.54 ± 0.22 TIP3P to SPC/E) and outside (1.73 ± 0.11 for

TIP4P to SPC/E and 2.28 ± 0.36 for TIP3P to SPC/E) of the membrane. This indicates that the relative effect of the water model choice on diffusivity is the same inside the membrane as it is in the bulk water. We note, however, that recent experimental results for water diffusivity within membranes, while similar in magnitude to those found here, are only reduced slightly from the diffusivity outside of the membrane. This surprising result may be a consequence of the difficulty in making these measurements, which depend on fitting various parameters to results from various techniques such as neutron scattering and were performed for aromatic polyamide membranes, not aromatic-aliphatic polyamide membranes considered here [58–60].

To explore the impact of the water model on the diffusivity further, we measure the average cohesive energy between water molecules, both inside the membrane and outside of it, over the last 4 ns of the equilibration, again using the NAMDEnergy tool. The water cohesive energies in the membrane are -5.45 ± 0.56, -4.59 ± 0.55, and -3.79 ± 0.84 kcal·mol^{-1} for SPC/E, TIP4P, and TIP3P, respectively. This can be compared to the cohesive energy of water molecules in a bulk water system containing the same number of water molecules but without the presence of a membrane, where the average bulk water cohesive energies are -9.98 ± 0.06, -9.76 ± 0.06, and -8.06 ± 0.06 kcal·mol^{-1} for SPC/E, TIP4P, and TIP3P, respectively. Although the energies are more similar for SPC/E and TIP4P in bulk water, the trend is preserved that SPC/E has the strongest self-interaction, which limits its mobility the most, both inside and outside of the membrane, resulting in the lowest diffusivity. TIP3P has the highest diffusivity because its cohesive energy is lowest both inside and outside of the membrane. Thus, the different cohesive energies for the water models likely explain the differences in the measured diffusivities in Fig. 6(a).

To confirm that the comparative relationship between the water models studied here is not affected by membrane charge concentration, we consider a set of simulations using pH ≈ 7 membrane at 300 K with Langevin damping parameter set at 0.2 ps^{-1}. The diffusivity within the pH ≈ 7 membrane is 50% to 80% higher than that in the pH ≈ 10 membrane. But the general trends for D_w and D_w^{mem} match those for the pH ≈ 10 membrane system: SPC/E has the lowest water diffusivity and TIP3P the highest.

As illustrated in Fig. 6(b), the negative linear slopes of ln(D) with 1/T for all water models are consistent with the Arrhenius relationship between D and temperature. Hence, although all water models manage to describe the qualitative relationship between diffusivity and temperature as well as reflect the reduced diffusivity in the membrane, the TIP4P model captures water self-diffusivity most accurately among all the water models investigated here.

Another important aspect is the temperature control scheme used in the simulations. For the Langevin thermostat used here, the damping coefficient γ determines the magnitude of random forces introduced into the system. The effect of Langevin damping coefficient, ranging from 0.1 to 10 ps^{-1}, on water diffusivity in the NF membrane systems at 300 K is shown in Fig. 7. The Langevin damping parameter γ has significant impact on the results, especially for bulk water. However, comparing to the horizontal band for experiments conducted at 298 K [53–56] indicates that TIP4P best matches the experimental results within the range of γ = 2 – 5 ps^{-1}, and TIP3P also reproduces reasonable results at γ = 5 – 10 ps^{-1}.

Based on the combined observations of the diffusivity dependence on temperature and the Langevin damping parameters, we conclude that TIP4P at γ = 2 – 5 ps^{-1} produces the most accurate description of water dynamics in terms of bulk water diffusivity. This result is consistent with a recent study indicating that for TIP4P/2005, γ = 1 – 5 ps^{-1} results in the most accurate description of water bulk viscosity [51]. The performance of the TIP4P model can most likely be attributed the more accurate electrostatic charge distribution of the 4-site TIP4P model compared to the 3-site models (see Fig.1). Furthermore, the TIP3P model was developed without including self-diffusion as part of the parameterization process, so its overestimate of D_w is not surprising [4].

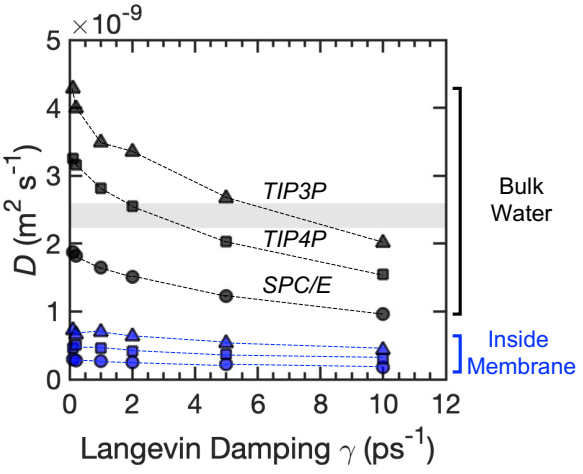

Figure 7: Diffusion coefficient D as a function of Langevin damping γ for SPC/E (○), TIP4P (□), and TIP3P (△) water models simulated at 300 K. Black symbols indicate D_w, and blue symbols indicate D_w^{mem}. Each data point is an average of 4 replicate simulations (error bars omitted for clarity). Experimental data range at 298 K is indicated by the shaded area [53–56]. (Color online.)

3.2.2. Water transport

We further quantify the impact of the water model on water transport in terms of the water flux using exactly the same pH ≈ 10 membrane nanostructure in all cases. The water flux at the molecular level is based on the net change in the number of water molecules in the permeate reservoir over the duration of the simulation normalized by the simulation time (20 ns) and the membrane surface area (27 nm^2). As shown in Fig. 8, number water flux increases linearly as temperature rises, which is consistent with experimental results [61–64]. Among all water models, TIP3P yields the largest number water flux at all temperatures and SPC/E

the smallest. At a given temperature, 300 K for example, TIP3P results in flux values twice as much as TIP4P and 7 times larger than SPC/E. To determine the most appropriate water model to use, we convert the number water flux to a macroscale representation indicated on the right vertical axis in Fig. 8. With transmembrane pressure and membrane thickness differences taken into account [28], experiments conducted at ambient temperature (293 K – 303 K) [65, 66] have equivalent flux values within the range of 0.013 m s^{-1} to 0.038 m s^{-1}, shown as the shaded box in Fig. 8. This suggests that flux values simulated using both TIP4P and TIP3P are consistent with the experiments. However, even with the same membrane structure in the simulations, flux values produced using TIP3P suggest a high-permeance membrane while TIP4P corresponds to low-permeance. Therefore, in addition to the membrane's intrinsic physical properties, the choice of water model has a large impact on the water transport performance.

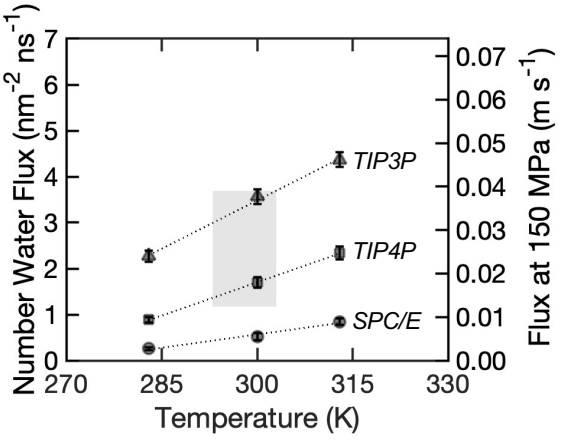

Figure 8: Number water flux as a function of temperature for SPC/E (○), TIP4P (□), and TIP3P (△) water models. Each standard error bar (smaller than the symbol in most cases) is for 4 replicate simulations. All simulations here use Langevin damping γ of 2 ps^{-1}. Experimental data range is indicated by the shaded area [65, 66].

To investigate the effect of the Langevin damping coefficient, the water flux is plotted against γ in Fig. 9. Water flux decreases as γ increases for all water models, as would be expected given the increasing bulk viscosity with increasing γ [51]. Based on experimental flux measurements around 300 K, indicated by the shaded region in Fig. 9, there are several acceptable combinations of TIP3P and TIP4P water models and Langevin damping values including the optimal conditions based diffusivity measurements in the previous subsection, TIP4P at $\gamma = 2 – 5$ ps^{-1}. Interestingly, the highest number water flux using TIP4P occurs at $\gamma = 0.2$ ps^{-1}, unlike other models where the highest flux is at the smallest value considered, $\gamma = 0.1$ ps^{-1}. However, we do not explore this further, given that the preferred values based on diffusivity results are $\gamma = 2 – 5$ ps^{-1}.

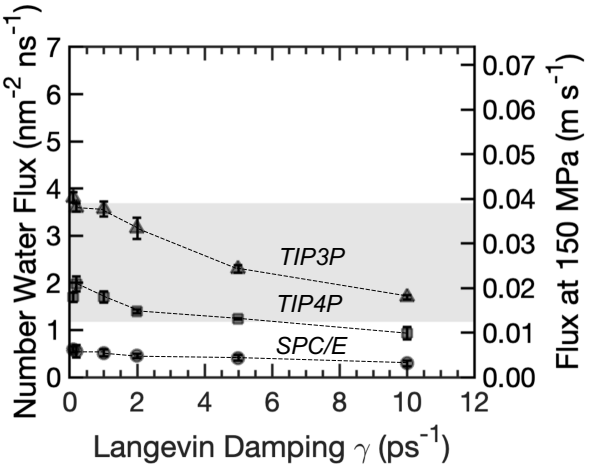

Figure 9: Number water flux as a function of Langevin damping γ for SPC/E (○), TIP4P (□), and TIP3P (△) water models simulated at 300 K. Each standard error bar (smaller than the symbol in most cases) is for 4 replicate simulations. Experimental data range is indicated by the shaded area [65, 66].

3.2.3. Flux and diffusivity correlation

So far, we conclude that among the water models investigated here, TIP4P best captures water self-diffusivity. However, many previous studies including our own use SPC/E or TIP3P, as indicated in Table 1. Hence, we assess the three models in terms of the relation between number water flux and D_w^{mem} (for water inside membrane), which we have shown previously to be linearly correlated [28]; that is, higher diffusivity and higher flux are both correlated with a looser membrane nanostructure, so diffusivity and flux are correlated with each other.

Fig. 10 shows the relation between water number flux and D_w^{mem} for our previous results (gray ×'s), which includes 220 simulations for 56 different neutral and charged NF membrane nanostructures using TIP3P at 300 K [28], and our new results for SPC/E, TIP4P, and TIP3P water models using a single membrane nanostructure (red data points). It is evident that the number water flux and membrane diffusivity simulated using different water models and at different temperatures or values for γ are still linearly correlated. While this reinforces the clear relationship between flux and water diffusivity regardless of simulation details including the specific water model that is used, it also emphasizes the impact of physical conditions (temperature) and simulation parameters (γ) in combination with the water model on the results. The broad range of data for diffusivity and water flux in our previous data (gray ×'s) can be directly attributed to the effect of the density of the membrane. High diffusivity and high flux correspond to a loose membrane nanostructure, while low diffusivity and low flux correspond to dense membrane nanostructure. The result is a linear relation between flux and diffusivity [28].

Consider first the effect of temperature in Fig. 10(a). A total of 12 simulations are included for each water model (4 replicates at each temperature), and the large range of data

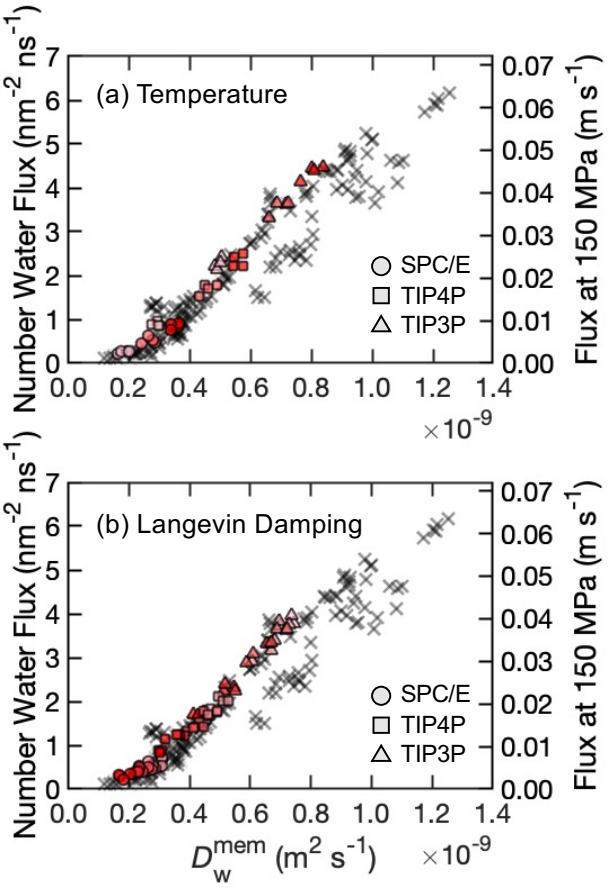

Figure 10: Number water flux as a function of diffusion coefficients D_w^{mem} for SPC/E (○), TIP4P (□), and TIP3P (△) water models with varying (a) temperature (283 K, 300 K, and 313 K) at $\gamma = 1$ ps^{-1} and (b) Langevin damping settings $0.1 \leq \gamma \leq 10$ ps^{-1} at 300 K. Darker red symbols indicate higher temperature or larger Langevin damping values. All previous data for neutral and charged membranes [28] are shown as gray ×. (Color online.)

for any particular water model is striking. It is clear that a wide range of diffusivities and water fluxes occur as a result of both differences in temperature (symbols with different red shading) and the variation from one replicate run to another (symbols with the same shading). Clearly, increased temperature (darker shading) results in increased diffusivity and flux, as would be expected for a looser membrane and higher water diffusivity at higher temperature. Of course, the choice of the water model also plays a very large role as previously indicated in Fig. 8. Nevertheless, all the data falls on the same linear correlation between water flux and density, regardless of water model, temperature, or variability between replicate runs. The impact of the simulation parameter, γ, is similar, shown in Fig. 10(b). That is, the linear relation between flux and diffusivity holds regardless of the specific value for γ and the water model that is used.

Hence, when studying the water transport within a polymeric membrane system, the wide range of water models used in previous studies (Table 1) is unlikely to have a detrimental effect on the qualitative aspects of the results. However, a realistic membrane model, the correct water model, and optimal MD simulation parameters are critical to consider when comparing results from one study to another and with quantitative experimental results.

3.3. Water model effect on water dynamics in salt solutions

The presence of ions can also affect water diffusivity, so we consider the water diffusivity with solutes, D_w^{sol}, for the SPC/E, TIP4P, and TIP3P water models for the simulation system shown in Fig. 3 with no membrane present. Consistent with pure water, TIP3P results in the largest D_w^{sol} and SPC/E the smallest, as shown in Fig. 11. The value for D_w^{sol} decreases with solute concentration for all solutions and water models studied here due to the interactions between ions and water molecules, consistent with experimental results (green data points) [67–69] and previous MD simulations for a single solute and concentration, 1 M NaCl [57]. In addition, for all solutions with non-zero concentrations, D_w^{sol} decreases following the order KCl > NaCl > $CaCl_2$ > $MgCl_2$ at any particular concentration. This is consistent with the reverse ordering for the cation Stokes radii [70–72], the hydrated cation radii [72], and the water mean lifetimes (τ_{water}) near the cations [73], all of which are reported to order as Mg^{2+} > Ca^{2+} > Na^+ > K^+. This suggests that the larger the cation hydrated radius or the longer the water molecules remain part of the solvation shell of the cation (larger τ_{water}), the lower the mobility of the water molecules due to ion-water interactions leading to smaller D_w^{sol}. Moreover, the disparity for D_w^{sol} among the different solutes becomes more pronounced at higher concentrations. The differences between the water models can again be related to the relative bulk water cohesive energies for the three water models, as described in the context of Fig. 6. Further note that it has been shown that charge scaling based on the experimental value of the dielectric constant improves the results for the dependence of D_w^{sol} on concentration, but it is not clear if this may be related to the differences between water models [57].

Experimental measurements of D_w^{sol} for the solutes considered here are sparse, but based on available experiments [68], there is no single water model that can best represent water dynamics for all solutes at all concentrations. However, TIP4P yields the closest D_w^{sol} for monovalent cation solutions at high concentration, while SPC/E better simulates the water dynamics for divalent cation solutions at low concentrations (< 0.5 M).

3.4. Water model effect on ion dynamics

3.4.1. Ion self-diffusivity

In addition to evaluating D_w^{sol} for ionic aqueous solutions, we also consider diffusion coefficients for the cations (D_{cation}) themselves in the same solutions with no membrane present. Fig. 12 shows D_{cation} as a function of solute concentration for the three different water models compared with the limited experimental data that is available for 1 gL^{-1} (0.013 M, 0.017 M, 0.009 M, and 0.011 M for KCl, NaCl,

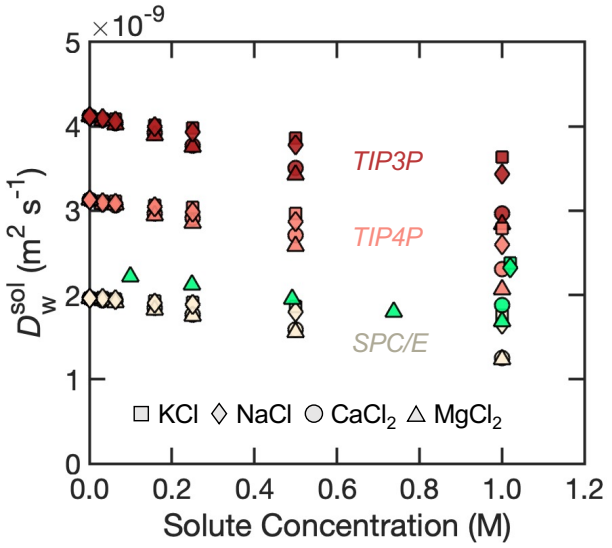

Figure 11: Water diffusion coefficients D_w^{sol} for SPC/E, TIP4P, and TIP3P (shades of red) as a function of solute concentration for KCl (□), NaCl (◇), $CaCl_2$ (○), and $MgCl_2$ (△) compared to experimental data [68] (green). (Color online.)

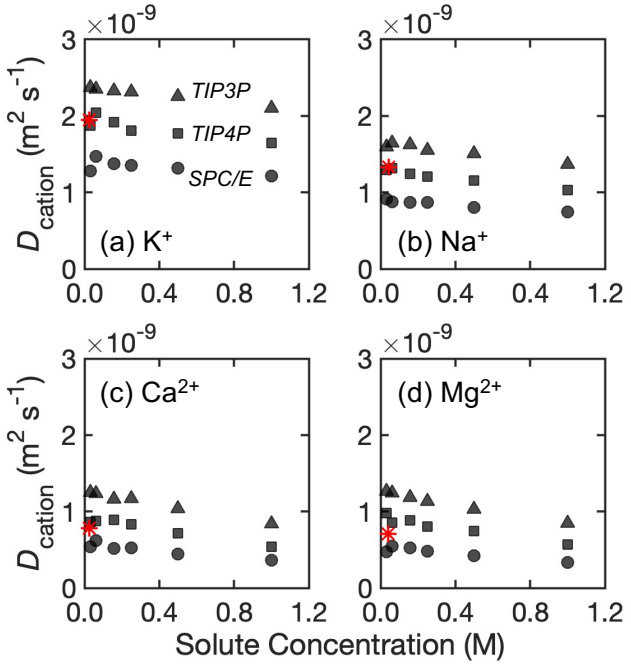

Figure 12: Diffusion coefficients D_{cation} for (a) K^+, (b) Na^+, (c) Ca^{2+}, and (d) Mg^{2+} using SPC/E (○), TIP4P (□), and TIP3P (△) as a function of solute concentration, compared to experimental data [70, 71] (*) . (Color online.)

$CaCl_2$, and $MgCl_2$, respectively) ionic solutions [70, 71]. Overall, TIP3P overpredicts and SPC/E underpredicts the cation self-diffusivity compared to the experiments. Note, however, that the most dilute solution simulated here (0.03 M) contains only one cation, which results in no ion-ion interactions in the periodic simulation domain. To verify the ion diffusivity in a dilute solution is not affected by the number of ions present, we performed simulations for NaCl and $CaCl_2$ where the system box size is doubled ($5.2 \times 5.2 \times 2.0$ nm^3 vs. $5.2 \times 5.2 \times 4.0$ nm^3), while maintaining the solution concentration at 0.03 M (two solute molecules in the larger system). Results show that the solute diffusivity does not change at constant concentration regardless of the number of solute molecules present. Nevertheless, among the water models considered here, TIP4P replicates cation dynamics the best based on the limited experimental results that are available for comparison. It is difficult to explain the differences in D_{cation} between the water models, although the success of the TIP4P water model is likely related to the superior electrostatic charge distribution of the TIP4P model to better reflect the polar nature of a water molecule.

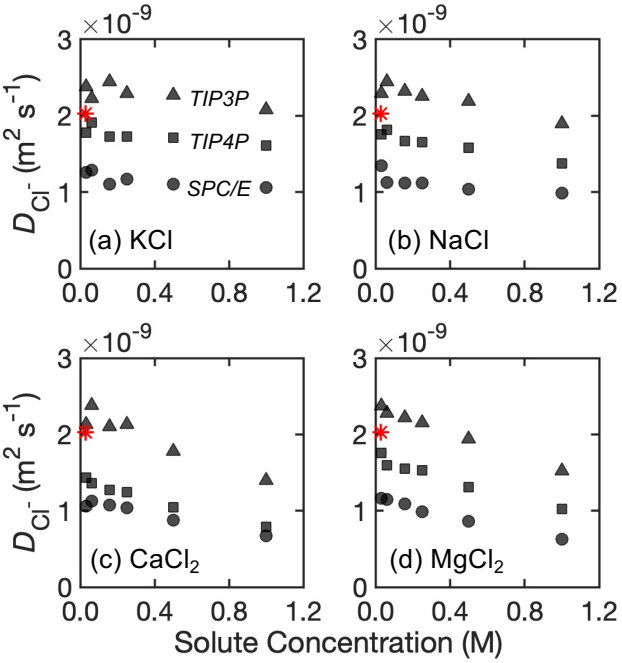

Figure 13: Diffusion coefficients D_{Cl^-} for Cl^- in (a) KCl, (b) NaCl, (c) $CaCl_2$, and (d) $MgCl_2$ using SPC/E (○), TIP4P (□), and TIP3P (△) as a function of solute concentration, compared to experimental data for a single measurement of Cl^- (see text) [70] (*) . (Color online.)

It is clear that D_{cation} generally decreases as solute concentration increases. Moreover, the monovalent cations, K^+ and Na^+, have larger diffusivity than the divalent ones, Ca^{2+} and Mg^{2+}. Furthermore, the ordering is consistent with the reverse ordering for the cation Stokes radii [70–72], the hydrated cation radii [72], and the water mean lifetimes (τ_{water}) near the cations [73], noted above, although Ca^{2+} and Mg^{2+} have almost identical diffusivity. Again, this suggests that the larger the cation hydrated radius or the longer the water molecules remain part of the solvation shell of the cation, the lower the mobility of the cation.

Likewise, diffusion coefficients for anion Cl^-, D_{Cl^-}, in different solutions follow similar patterns, as shown in Fig. 13. TIP3P yields the largest D_{Cl^-} among all three water models, and SPC/E the smallest. In general, D_{Cl^-} decreases as

concentration increases, but the decrease is steeper with the ordering $Mg^{2+} \approx Ca^{2+} > Na^{+} > K^{+}$. Again this is probably related to cation hydration noted above also affecting the anion diffusion at higher concentration. However, at low concentrations, D_{Cl^-} is very similar regardless of the cation for each of the three water models. The exception is TIP4P for $CaCl_2$, which we return to shortly.

Since there is only one experimental result that we can find for D_{Cl^-} [70] (although it is not clear if this corresponds to KCl, NaCl, or $CaCl_2$ in the experimental study), we use this single experimental D_{Cl^-} value to compare with our computational results. The TIP3P and TIP4P models appear to work best when comparing simulation and experimental results for D_{Cl^-}, although TIP3P over-predicts and TIP4P underpredicts D_{Cl^-}, except for $CaCl_2$ where TIP3P works best. Hence, the best water model to simulate Cl^- dynamics depends on the salt solution, and there appears to be no one-fits-all water model to characterize Cl^- dynamics. We note that D_{K^+}, D_{Na^+}, and D_{Cl^-} obtained here for 1 M solutions using the SPC/E and TIP3P models average about 40% lower than those found in previous MD simulation [57], although this study use a different thermostat and simulation package as well as a very small simulation volume, as noted in Section 3.2.1.

3.4.2. Ion-water coordination number

As we alluded to earlier, an important metric to describe water dynamics near ions is the water coordination number (WCN) of the hydrated ion, which is the number of water molecules in the first solvation shell. Since multiple solute concentrations are used, we consider the WCN averaged over all concentrations with their standard error, as shown in Fig. 14, and compare to experimental measurements [74–81].

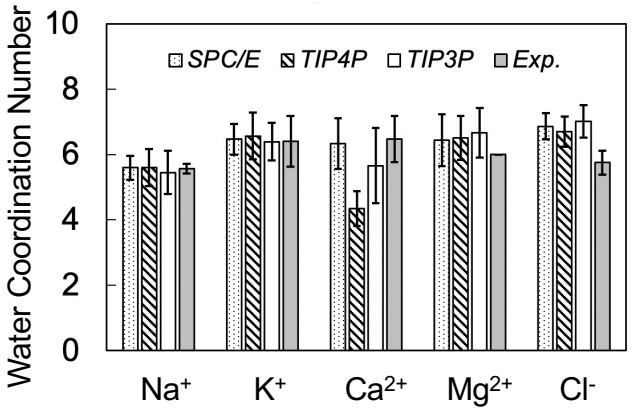

Figure 14: Water coordination number (WCN) for K^+, Na^+, Ca^{2+}, Mg^{2+}, and Cl^- found using SPC/E, TIP4P, and TIP3P, compared with experimental data [74–81].

Overall, the WCN for all ions except Ca^{2+} are within a similar range among SPC/E, TIP4P, and TIP3P, and the results match experiments reasonably well. Hence, it is hard to select one water model over another for Na^+, K^+, Mg^{2+}, or Cl^-. However, for Ca^{2+}, the WCN for SPC/E matches experimental results best. On the other hand, for Cl^- and, to a smaller extent, Mg^{2+}, all water models overestimate the WCN by similar amount compared to the experiments. Therefore, based on the WCN measurement alone, none of the water models stand out, and for reliable WCN results for Ca^{2+}, SPC/E is optimal.

4. Conclusions

While realistic membrane structures are crucial to exploring water and ion transport using MD simulations, we show here that water models and simulation parameters also affect water transport and ion dynamics significantly. Previous studies of various water models have provided only minimal insight in explaining such differences for pure water [4, 10–12, 57], let alone when the water model interacts with atomistic models for the membrane or ions. In this study, we connect the differences between the water models to specific aspects of the water model interactions with the membrane polymers and the intrinsic cohesive energy between water molecules. Interaction energies between the membrane and water molecules indicate that SPC/E has the strongest affinity with the membrane while TIP3P has the weakest interaction. This is also consistent with the cohesive energy between water molecules themselves, where SPC/E self-associates the most and TIP3P the least. Hence, regardless of membrane charge concentration (pH ≈7 or pH ≈10), the water model with the largest cohesive energy and interaction with the membrane, SPC/E, has the least mobility to traverse through the membrane, while the opposite occurs for TIP3P, thus explaining the trend for water transport and diffusivity.

To aid future researchers in deciding which water model to use, we rate each water model qualitatively in Table 4 based on the metrics discussed in previous sections. The upper three metrics correspond to water dynamics in membrane systems, and the lower three describe ion dynamics in salt solutions. Based on this table, we conclude that overall the TIP4P water model renders the most accurate description of both water and ion dynamics. Nevertheless, previous MD studies using other water models are likely to still provide useful comparative results for conditions using the same water model. However, caution is advised when making detailed quantitative comparisons between simulations using different water models.

Table 4
Evaluation of SPC/E, TIP4P, and TIP3P. (Color online.)

Metric	SPC/E	TIP4P	TIP3P
Water D (Fig. 6)	□	○	×
Water flux (Figs. 8, 9)	×	○	○
Water D in solution (Fig. 11)	○	□	×
Cation D (Fig. 12)	□	○	×
Anion D (Fig. 13)	×	□	○
WCN (Fig. 14)	○	□	○

Legend: × – poor □ – fair ○ – good

Returning to the issue of simulation time mentioned in the Introduction, it is important to note that using the 4-site TIP4P water model requires longer simulation times than the 3-site SPC/E and TIP3P models. Based on our experience running simulations on a high-performance workstation (40 CPUs with an NVIDIA® Quadro® GV100 GPU), we find that simulations of the magnitude described in this paper take approximately 20 – 30% more wall clock time for TIP4P than for the other two water models.

Of course, there may be other combinations of conditions and water models for MD simulations of water filtration membranes that can satisfactorily reproduce actual water and ion dynamics. However, this study provides qualitative and quantitative comparisons of the three most common water models, which will be useful for future MD simulations of polymeric membranes.

Acknowledgments

We are grateful for several helpful discussions with Steve Jons, Jeff Wilbur, Tirtha Chatterjee, and Toni Bechtel at DuPont Water Solutions. This material is based upon work supported by the National Science Foundation under Grant No. CBET-1840816.

References

[1] H. F. Ridgway, J. Orbell, S. Gray, Molecular simulations of polyamide membrane materials used in desalination and water reuse applications: Recent developments and future prospects, Journal of Membrane Science 524 (2017) 436–448.

[2] M. Heiranian, R. M. DuChanois, C. L. Ritt, C. Violet, M. Elimelech, Molecular simulations to elucidate transport phenomena in polymeric membranes, Environmental Science and Technology 56 (6) (2022) 3313–3323.

[3] M. Paul, S. D. Jons, Chemistry and fabrication of polymeric nanofiltration membranes: A review, Polymer 103 (2016) 417–456.

[4] S. P. K. Pathirannahalage, N. Meftahi, A. Elbourne, A. C. G. Weiss, C. F. McConville, A. Padua, D. A. Winkler, M. C. Gomes, T. L. Greaves, T. C. Le, Q. A. Besford, A. J. Christofferson, Systematic comparison of the structural and dynamic properties of commonly used water models for molecular dynamics simulations, Journal of Chemical Information and Modeling 61 (2021) 4521–4536.

[5] H. Berendsen, J. Postma, W. Van Gunsteren, J. Hermans, Intermolecular forces, edited by: Pullman, B. 331–342 (1981).

[6] H. Berendsen, J. Grigera, T. Straatsma, The missing term in effective pair potentials, Journal of Physical Chemistry 91 (24) (1987) 6269–6271.

[7] Y. Wu, H. L. Tepper, G. A. Voth, Flexible simple point-charge water model with improved liquid-state properties, Journal of Chemical Physics 124 (2) (2006) 024503.

[8] W. L. Jorgensen, J. Chandrasekhar, J. D. Madura, R. W. Impey, M. L. Klein, Comparison of simple potential functions for simulating liquid water, Journal of Chemical Physics 79 (2) (1983) 926–935.

[9] W. L. Jorgensen, J. D. Madura, Temperature and size dependence for Monte Carlo simulations of TIP4P water, Molecular Physics 56 (1985) 1381–1392.

[10] M. W. Mahoney, W. L. Jorgensen, A five-site model for liquid water and the reproduction of the density anomaly by rigid, nonpolarizable potential functions, Journal of Chemical Physics 112 (20) (2000) 8910–8922.

[11] P. Mark, L. Nilsson, Structure and dynamics of the TIP3P, SPC, and SPC/E water models at 298 K, Journal of Physical Chemistry A 105 (43) (2001) 9954–9960.

[12] J. Zielkiewicz, Structural properties of water: Comparison of the SPC, SPC/E, TIP4P, and TIP5P models of water, Journal of Chemical Physics 123 (10) (2005) 104501.

[13] V. Prasad, S. K. Kannam, R. Hartkamp, S. P. Sathian, Water desalination using graphene nanopores: influence of the water models used in simulations, Physical Chemistry Chemical Physics 20 (23) (2018) 16005–16011.

[14] L. Liu, G. Patey, Simulations of water transport through carbon nanotubes: how different water models influence the conduction rate, Journal of Chemical Physics 141 (18) (2014) 18C518.

[15] A. Srivastava, S. Malik, A. Debnath, Heterogeneity in structure and dynamics of water near bilayers using TIP3P and TIP4P/2005 water models, Chemical Physics 525 (2019) 110396.

[16] Y. Xiang, Y. Liu, B. Mi, Y. Leng, Hydrated polyamide membrane and its interaction with alginate: a molecular dynamics study, Langmuir 29 (37) (2013) 11600–11608.

[17] Y. Xiang, Y. Liu, B. Mi, Y. Leng, Molecular dynamics simulations of polyamide membrane, calcium alginate gel, and their interactions in aqueous solution, Langmuir 30 (30) (2014) 9098–9106.

[18] Y. Xiang, R.-G. Xu, Y. Leng, Molecular dynamics simulations of a poly (ethylene glycol)-grafted polyamide membrane and its interaction with a calcium alginate gel, Langmuir 32 (18) (2016) 4424–4433.

[19] V. Kolev, V. Freger, Molecular dynamics investigation of ion sorption and permeation in desalination membranes, Journal of Physical Chemistry B 119 (44) (2015) 14168–14179.

[20] J. Muscatello, E. Müller, A. Mostofi, A. Sutton, Multiscale molecular simulations of the formation and structure of polyamide membranes created by interfacial polymerization, Journal of Membrane Science 527 (2017) 180–190.

[21] E. Harder, D. E. Walters, Y. D. Bodnar, R. S. Faibish, B. Roux, Molecular dynamics study of a polymeric reverse osmosis membrane, Journal of Physical Chemistry B 113 (30) (2009) 10177–10182.

[22] V. Kolev, V. Freger, Hydration, porosity and water dynamics in the polyamide layer of reverse osmosis membranes: A molecular dynamics study, Polymer 55 (6) (2014) 1420–1426.

[23] Y. Luo, E. Harder, R. S. Faibish, B. Roux, Computer simulations of water flux and salt permeability of the reverse osmosis FT-30 aromatic polyamide membrane, Journal of Membrane Science 384 (1-2) (2011) 1–9.

[24] M. Shen, S. Keten, R. M. Lueptow, Dynamics of water and solute transport in polymeric reverse osmosis membranes via molecular dynamics simulations, Journal of Membrane Science 506 (2016) 95–108.

[25] M. Shen, S. Keten, R. M. Lueptow, Rejection mechanisms for contaminants in polyamide reverse osmosis membranes, Journal of Membrane Science 509 (2016) 36–47.

[26] H. Zhang, M. S. Wu, K. Zhou, A. W.-K. Law, Molecular insights into the composition–structure–property relationships of polyamide thin films for reverse osmosis desalination, Environmental Science & Technology 53 (11) (2019) 6374–6382.

[27] M. S. Jahan Sajib, Y. Wei, A. Mishra, L. Zhang, K.-I. Nomura, R. K. Kalia, P. Vashishta, A. Nakano, S. Murad, T. Wei, Atomistic simulations of biofouling and molecular transfer of a cross-linked aromatic polyamide membrane for desalination, Langmuir 36 (26) (2020) 7658–7668.

[28] S. Liu, S. Ganti-Agrawal, S. Keten, R. M. Lueptow, Molecular insights into charged nanofiltration membranes: Structure, water transport, and water diffusion, Journal of Membrane Science 644 (2022) 120057.

[29] W. Zhang, R. Chu, W. Shi, Y. Hu, Quantitively unveiling the activity-structure relationship of polyamide membrane: A molecular dynamics simulation study, Desalination 528 (2022) 115640.

[30] Z. E. Hughes, J. D. Gale, A computational investigation of the properties of a reverse osmosis membrane, Journal of Materials Chemistry 20 (36) (2010) 7788–7799.

[31] Z. E. Hughes, J. D. Gale, Molecular dynamics simulations of the interactions of potential foulant molecules and a reverse osmosis membrane, Journal of Materials Chemistry 22 (1) (2012) 175–184.

[32] M. Ding, A. Ghoufi, A. Szymczyk, Molecular simulations of polyamide reverse osmosis membranes, Desalination 343 (2014) 48–53.
[33] M. Ding, A. Szymczyk, F. Goujon, A. Soldera, A. Ghoufi, Structure and dynamics of water confined in a polyamide reverse-osmosis membrane: A molecular-simulation study, Journal of Membrane Science 458 (2014) 236–244.
[34] M. Ding, A. Szymczyk, A. Ghoufi, On the structure and rejection of ions by a polyamide membrane in pressure-driven molecular dynamics simulations, Desalination 368 (2015) 76–80.
[35] M. Ding, A. Szymczyk, A. Ghoufi, Hydration of a polyamide reverse-osmosis membrane, Journal of Membrane Science 501 (2016) 248–253.
[36] T. P. Liyana-Arachchi, J. F. Sturnfield, C. M. Colina, Ultrathin molecular-layer-by-layer polyamide membranes: insights from atomistic molecular simulations, Journal of Physical Chemistry B 120 (35) (2016) 9484–9494.
[37] S. Nosé, A unified formulation of the constant temperature molecular dynamics methods, Journal of Chemical Physics 81 (1) (1984) 511–519.
[38] W. G. Hoover, Canonical dynamics: Equilibrium phase-space distributions, Physical Review A 31 (3) (1985) 1695.
[39] D. J. Evans, B. L. Holian, The Nosé-Hoover thermostat, Journal of Chemical Physics 83 (8) (1985) 4069–4074.
[40] H. J. Berendsen, J. v. Postma, W. F. Van Gunsteren, A. DiNola, J. R. Haak, Molecular dynamics with coupling to an external bath, Journal of Chemical Physics 81 (8) (1984) 3684–3690.
[41] M. C. Wang, G. E. Uhlenbeck, On the theory of the brownian motion II, Reviews of Modern Physics 17 (2-3) (1945) 323.
[42] G. Bussi, D. Donadio, M. Parrinello, Canonical sampling through velocity rescaling, Journal of Chemical Physics 126 (1) (2007) 014101.
[43] J. C. Phillips, R. Braun, W. Wang, J. Gumbart, E. Tajkhorshid, E. Villa, C. Chipot, R. D. Skeel, L. Kale, K. Schulten, Scalable molecular dynamics with NAMD, Journal of Computational Chemistry 26 (16) (2005) 1781–1802.
[44] J. C. Phillips, D. J. Hardy, J. D. Maia, J. E. Stone, J. V. Ribeiro, R. C. Bernardi, R. Buch, G. Fiorin, J. Hénin, W. Jiang, et al., Scalable molecular dynamics on CPU and GPU architectures with NAMD, Journal of Chemical Physics 153 (4) (2020) 044130.
[45] J. Wang, R. M. Wolf, J. W. Caldwell, P. A. Kollman, D. A. Case, Development and testing of a general AMBER force field, Journal of Computational Chemistry 25 (9) (2004) 1157–1174.
[46] J.-P. Ryckaert, G. Ciccotti, H. J. Berendsen, Numerical integration of the Cartesian equations of motion of a system with constraints: Molecular Dynamics of n-alkanes, Journal of Computational Physics 23 (3) (1977) 327–341.
[47] T. Darden, D. York, L. Pedersen, Particle Mesh Ewald: An Nlog(N) method for Ewald sums in large systems, Journal of Chemical Physics 98 (12) (1993) 10089–10092.
[48] A. D. MacKerell Jr, D. Bashford, M. Bellott, R. L. Dunbrack Jr, J. D. Evanseck, M. J. Field, S. Fischer, J. Gao, H. Guo, S. Ha, et al., All-atom empirical potential for molecular modeling and dynamics studies of proteins, Journal of Physical Chemistry B 102 (18) (1998) 3586–3616.
[49] O. Coronell, M. I. González, B. J. Mariñas, D. G. Cahill, Ionization behavior, stoichiometry of association, and accessibility of functional groups in the active layers of reverse osmosis and nanofiltration membranes, Environmental Science & Technology 44 (17) (2010) 6808–6814.
[50] C. L. Ritt, J. R. Werber, M. Wang, Z. Yang, Y. Zhao, H. J. Kulik, M. Elimelech, Ionization behavior of nanoporous polyamide membranes, Proceedings of the National Academy of Sciences 117 (48) (2020) 30191–30200.
[51] R. Hafner, G. Guevara-Carrion, J. Vrabec, P. Klein, Sampling the bulk viscosity of water with molecular dynamics simulation in the canonical ensemble, Journal of Physical Chemistry B (2022).
[52] D. Beglov, B. Roux, Finite representation of an infinite bulk system: solvent boundary potential for computer simulations, Journal of Chemical Physics 100 (12) (1994) 9050–9063.
[53] J. H. Wang, Self-diffusion coefficients of water, Journal of Physical Chemistry 69 (12) (1965) 4412–4412.
[54] K. T. Gillen, D. Douglass, M. Hoch, Self-diffusion in liquid water to -31°C, Journal of Chemical Physics 57 (12) (1972) 5117–5119.
[55] R. Mills, Self-diffusion in normal and heavy water in the range 1-45°, Journal of Physical Chemistry 77 (5) (1973) 685–688.
[56] K. Krynicki, C. D. Green, D. W. Sawyer, Pressure and temperature dependence of self-diffusion in water, Faraday Discussions of the Chemical Society 66 (1978) 199–208.
[57] Z. Kann, J. Skinner, A scaled-ionic-charge simulation model that reproduces enhanced and suppressed water diffusion in aqueous salt solutions, Journal of Chemical Physics 141 (10) (2014) 104507.
[58] E. P. Chan, B. R. Frieberg, K. Ito, J. Tarver, M. Tyagi, W. Zhang, E. B. Coughlin, C. M. Stafford, A. Roy, S. Rosenberg, C. L. Soles, Insights into the water transport mechanism in polymeric membranes from neutron scattering, Macromolecules 53 (2020) 1443–1450.
[59] F. Foglia, B. Frick, M. Nania, A. G. Livingston, J. T. Cabral, Multimodal confined water dynamics in reverse osmosis polyamide membranes, Nature Communications 13 (2022) 2809.
[60] T. E. Culp, B. Khara, K. P. Brickey, M. Geitner, T. J. Zimudzi, J. D. Wilbur, S. D. Jons, A. Roy, M. Paul, B. Ganapathysubramanian, A. L. Zydney, M. Kumar, E. D. Gomez, Nanoscale control of internal inhomogeneity enhances water transport in desalination membranes, Science 371 (2021) 72–75.
[61] J. Schaep, B. Van der Bruggen, S. Uytterhoeven, R. Croux, C. Vandecasteele, D. Wilms, E. Van Houtte, F. Vanlerberghe, Removal of hardness from groundwater by nanofiltration, Desalination 119 (1-3) (1998) 295–301.
[62] X. Jian, Y. Dai, G. He, G. Chen, Preparation of UF and NF poly (phthalazine ether sulfone ketone) membranes for high temperature application, Journal of Membrane Science 161 (1-2) (1999) 185–191.
[63] M. Mänttäri, A. Pihlajamäki, E. Kaipainen, M. Nyström, Effect of temperature and membrane pre-treatment by pressure on the filtration properties of nanofiltration membranes, Desalination 145 (1-3) (2002) 81–86.
[64] X. Jin, A. Jawor, S. Kim, E. M. Hoek, Effects of feed water temperature on separation performance and organic fouling of brackish water RO membranes, Desalination 239 (1-3) (2009) 346–359.
[65] V. Freger, Swelling and morphology of the skin layer of polyamide composite membranes: an atomic force microscopy study, Environmental Science & Technology 38 (11) (2004) 3168–3175.
[66] H. Q. Dang, W. E. Price, L. D. Nghiem, The effects of feed solution temperature on pore size and trace organic contaminant rejection by the nanofiltration membrane NF270, Separation and Purification Technology 125 (2014) 43–51.
[67] J. S. Kim, Z. Wu, A. R. Morrow, A. Yethiraj, A. Yethiraj, Self-diffusion and viscosity in electrolyte solutions, Journal of Physical Chemistry B 116 (39) (2012) 12007–12013.
[68] K. Müller, H. Hertz, A parameter as an indicator for water-water association in solutions of strong electrolytes, Journal of Physical Chemistry 100 (4) (1996) 1256–1265.
[69] P. Ben Ishai, E. Mamontov, J. D. Nickels, A. P. Sokolov, Influence of ions on water diffusion□ a neutron scattering study, Journal of Physical Chemistry B 117 (25) (2013) 7724–7728.
[70] G. Bargeman, J. Vollenbroek, J. Straatsma, C. Schroën, R. Boom, Nanofiltration of multi-component feeds. interactions between neutral and charged components and their effect on retention, Journal of Membrane Science 247 (1-2) (2005) 11–20.
[71] G. Bargeman, J. Westerink, C. Manuhutu, A. Ten Kate, The effect of membrane characteristics on nanofiltration membrane performance during processing of practically saturated salt solutions, Journal of Membrane Science 485 (2015) 112–122.
[72] E. R. Nightingale, Phenomenological theory of ion solvation. effective radii of hydrated ions, Journal of Physical Chemistry 63 (1959) 1381–1387.
[73] L. Helm, A. E. Merbach, Inorganic and bioinorganic solvent exchange mechanisms, Chemical Reviews 105 (6) (2005) 1923–1960.

[74] L. X. Dang, J. E. Rice, J. Caldwell, P. A. Kollman, Ion solvation in polarizable water: molecular dynamics simulations, Journal of the American Chemical Society 113 (7) (1991) 2481–2486.
[75] E. Clementi, R. Barsotti, Study of the structure of molecular complexes. coordination numbers for Li^+, Na^+, K^+, F^- and Cl^- in water, Chemical Physics Letters 59 (1) (1978) 21–25.
[76] G. Neilson, J. Enderby, Neutron and x-ray diffraction studies of concentrated aqueous electrolyte solutions, Annual Reports Section C (Physical Chemistry) 76 (1979) 185–220.
[77] H. Ohtaki, T. Radnai, Structure and dynamics of hydrated ions, Chemical Reviews 93 (3) (1993) 1157–1204.
[78] N. Hewish, G. Neilson, J. Enderby, Environment of Ca^{2+} ions in aqueous solvent, Nature 297 (5862) (1982) 138–139.
[79] S. Cummings, J. Enderby, R. Howe, Ion hydration in aqueous $CaCl_2$ solutions, Journal of Physics C: Solid State Physics 13 (1) (1980) 1.
[80] H. J. Kulik, N. Marzari, A. A. Correa, D. Prendergast, E. Schwegler, G. Galli, Local effects in the X-ray absorption spectrum of salt water, Journal of Physical Chemistry B 114 (29) (2010) 9594–9601.
[81] P. E. Mason, L. Tavagnacco, M.-L. Saboungi, T. Hansen, H. E. Fischer, G. W. Neilson, T. Ichiye, J. W. Brady, Molecular dynamics and neutron scattering studies of potassium chloride in aqueous solution, Journal of Physical Chemistry B 123 (50) (2019) 10807–10813.